Received October 2001
Revised June 2003
Accepted August 2003

Numerical study of active shock control for transonic aerodynamics

N. Qin
Department of Mechanical Engineering, University of Sheffield, Sheffield, UK
Y. Zhu
Department of Mechanical Engineering, Brunel University, Uxbridge, UK
S.T. Shaw
College of Aeronautics, Cranfield University, Bedford, UK

Keywords *Aerodynamics, Waveforms, Flow, Differential equations, Numerical analysis*

Abstract *In this paper, the effectiveness of a number of active devices for the control of shock waves on transonic aerofoils is investigated using numerical solutions of the Reynolds-averaged Navier-Stokes equations. A brief description of the flow model and the numerical method is presented including, in particular, the boundary condition modelling and the numerical treatment for surface mass transfer. Comparisons with experimental data have been made where possible to validate the numerical study before some systematic numerical simulations for a parametric study. The effects of surface suction, blowing, and local modification of the surface contour (bump) on aerofoil aerodynamic performance have been studied extensively regarding the control location, the mass flow strength and the bump height. The numerical simulations highlight the benefits and drawbacks of the various control devices for transonic aerodynamic performance and identify the key design parameters for optimisation.*

1. Introduction

For aircraft flying at high subsonic Mach numbers, local pockets of supersonic flow develop over the lifting surfaces that are usually terminated by a shock wave. Associated with the appearance of the shock wave is an increase in drag, resulting from the entropy losses due to the shock wave itself (wave drag) and from the corresponding shock-boundary layer interaction (increase in skin friction). For large transport aircraft, control of the shock can reduce the drag substantially at the cruise condition with obvious implications for fuel economy and range. In addition, control of shock strength and buffet provides scope for noise reduction on rotorcraft and improved agility for military aircraft. The formation of shock waves, their interaction with the boundary layer and their control have been the subject of extensive research (Pearcey, 1961; Delery, 1985, 1999).

Early attempts to control the phenomena relied heavily on careful aerofoil design and the use of passive devices to re-energise the boundary layer ahead of the shock. Pearcey (1961) describes in detail the application of vane vortex

International Journal of Numerical Methods for Heat & Fluid Flow
Vol. 14 No. 4, 2004
pp. 444-466

0961-5539
DOI 10.1108/09615530410532240

generators to the problem of shock control on transonic wings. The control mechanism of vortex generators relies on the strong discrete vortices produced by the vanes to mix high-energy fluid from the freestream with the retarded fluid in the outer regions of the boundary layer. Using this technique shock induced boundary layer separation can be suppressed at the cost of a viscous drag penalty.

Alternatively, control of the shock can be achieved using the difference in pressure before and after the shock to produce natural flow circulation (Delery, 1999). This can be obtained by placing a cavity and porous plate at the foot of the shock. Experimental tests indicate that significant reductions in wave drag can be achieved due to the weakening of the shock wave by the pre-compression of the distorted displacement surface ahead of the shock position. However, in almost all of the cases studied, there is an increase in total drag due to the accompanying increase in skin friction in the control region.

While the use of passive devices for flow control has been demonstrated to improve the aerodynamic performance at the design point, the effect at off-design conditions is often detrimental. To overcome this problem, attention has recently shifted towards the use of active flow management techniques, in which the control device can be "switched on" to improve the performance locally within the flight envelope and "switched off" when not required. Two main control strategies can be identified; surface mass transfer and local modification of the surface contour.

1.1 Surface mass transfer

The basic principle underlying the control of shock boundary layer interaction is to increase the overall energy of the boundary layer, so that it is better able to negotiate the strong adverse pressure gradient across the shock. This can be achieved more readily by mass injection or mass removal. Mass removal by suction at the aerofoil surface was proposed by Regenscheit (1941) and has been studied extensively as a means of controlling shock wave-boundary layer interaction (Pearcey, 1961; Smith and Walker, 1960). Smith and Walker showed that lift could be increased by application of strong suction in the interaction region. More recently, computational studies by Qin and Zhu (1999) and Qin *et al.* (1999) have shown that application of suction in the strong adverse pressure gradient region delays separation and increases lift, however this is achieved with an increase in shock strength and increased drag.

Alternatively, momentum can be injected directly into the boundary layer through the surface of the aerofoil. This modifies the boundary layer displacement in such a way that the flow ahead of the shock must negotiate a "viscous ramp". The acceleration of the inviscid outer flow over the disturbed boundary layer ahead of the shock induces weak compression waves that soften the adverse pressure gradient experienced by the boundary layer in the interaction region. Mass injection for shock control was investigated

experimentally by Chen *et al.* (1989) and Wong (1977). Zhu (2000) and Zhu and Qin (1999) investigated the performance of slot blowing using solutions of the Navier-Stokes equations.

1.2 Local modification of the surface contour

Ashill and Fulker (1999) and Ashill *et al.* (1996) proposed devices which utilise local displacements of the aerofoil surface geometry for effective control of the shock and shock-boundary layer interaction. The surface bump can be viewed as a replacement of the "air bump" generated over the porous surface in the passive flow control case, mentioned earlier. Such devices accelerate the flow over the upstream face of the bump or ramp, inducing compression waves ahead of the shock. This results in a substantial reduction in wave drag, as the flow now negotiates a system of weaker compressions rather than a single strong normal shock. However, the presence of the device increases the momentum loss of the downstream boundary layer resulting in increased viscous drag, but this increase in skin-friction can be amply offset by the change in wave drag, leading to an overall drag reduction. Zhu (2000) performed an extensive parametric study on ramps and bumps using solutions of the Navier-Stokes equations. The shock bump can be viewed as being "active" in the sense that it may be deployed when required by active change of the local wing geometry although a fixed device may also prove to be beneficial.

2. Physical model and solution method

2.1 Governing equations

The physical problem under consideration is that of compressible viscous airflow involving shock waves, shear layers (including boundary layers) and their interactions. The mathematical model used is the two-dimensional compressible thin-layer Navier-Stokes equations. In turbulent cases, the Reynolds averaged Navier-Stokes equations are used with either the Baldwin and Lomax (1978) algebraic turbulence model or the two equation k-ω turbulence model.

The law of conservation of mass, momentum and energy over an area S bounded by a contour line l can be expressed in integral form as:

$$\frac{\partial}{\partial t}\int_S \mathbf{q}\,\mathrm{d}S + \int_l (\mathbf{H}\cdot\mathbf{n})\,\mathrm{d}l = 0 \tag{1}$$

where $\mathbf{q}$ is the conservative variable vector and $\mathbf{n}$ is the outward pointing unit vector normal to the line l. The flux tensor $\mathbf{H}$ can be written in terms of the Cartesian flux including inviscid and viscous contributions.

2.2 Surface mass transfer model

The effect of mass transfer at the wall is modelled in the Baldwin-Lomax turbulence model using the modification to the Van Driest factor proposed by Cebeci (1970).

$$A^+ = 26\left\{\exp\left(11.8v_{\mathrm{w}}^+\right) - \frac{p^+}{v_{\mathrm{w}}^+}\left[\exp\left(11.8v_{\mathrm{w}}^+\right) - 1\right]\right\}^{-1/2} \tag{2}$$

in which

$$p^+ = -\frac{(\mathrm{d}p/\mathrm{d}\xi)_{\mathrm{w}}\mu_{\mathrm{w}}}{\rho_{\mathrm{w}}^2(u_{\mathrm{w}}^*)^3} \tag{3}$$

and

$$v_{\mathrm{w}}^+ = \frac{v_{\mathrm{w}}}{u_{\mathrm{w}}^*} \tag{4}$$

$(\mathrm{d}p/\mathrm{d}\xi)_{\mathrm{w}}$ is the pressure gradient at the wall in the streamwise direction, μ_{w} is the molecular viscosity at the wall, and u_{w}^* is the friction velocity given.

2.3 Numerical method

The equations are discretised by a cell-centred finite-volume method, where numerical fluxes at each cell-cell interfaces are calculated and used to update the solution at the cell centres. Derivatives in the viscous flux at the interfaces are evaluated by creating auxiliary cells and implementing the Gauss theorem. The inviscid or convective fluxes need special attention for both shock waves and boundary layers. Shock waves are considered as discontinuities and therefore, are weak solutions of the governing equations. Conservative discretisation and approximate Riemann solvers for the convective flux evaluation provide a methodology for sharp shock capturing capability. The shock capturing method also needs to resolve the boundary layers by limiting the numerical dissipation so that the physical viscosity is properly modelled, rather than overshadowed by the numerical viscosity. Some details of the numerical aspects are given below and further details can be found in the study of Qin *et al.* (2000).

2.3.1 Approximate Riemann solver. The convective numerical flux at the cell interface is evaluated using Osher's approximate Riemann solver, which can be written as:

$$\tilde{E}_{i+\frac{1}{2},j} = \frac{1}{2}[\bar{E}(Q^{\mathrm{L}}) + \bar{E}(Q^{\mathrm{R}})] - \frac{1}{2}\int_{Q^{\mathrm{L}}}^{Q^{\mathrm{R}}}\left|\frac{\partial\bar{E}}{\partial Q}\right|\mathrm{d}Q \tag{5}$$

where $\bar{E}$ is the transformed flux in ξ direction and Q^{L}, Q^{R} the flow states on the left and right sides of the interface, respectively. The integration in the last term on the right hand side in the state space is carried out using a natural ordering of the sub-paths parallel to the eigenvectors of the flux Jacobian $\partial\bar{E}/\partial Q$.

2.3.2 High order variable extrapolation scheme. To attain higher order accuracy, the van Leer's variable extrapolation scheme is used. This means

that a linear or higher order approximation of the solution is used on each cell to calculate the interface values, rather than a piecewise constant solution.

In the equation below, Δ_- and Δ_+ are the forward and backward difference operators, respectively, and q is the column vector for the primitive variables. The parameter, κ, determines the spatial accuracy of the interpolation. Here, $\kappa = 1/3$ is chosen for a third order upwind biased scheme.

The scheme is implemented as:

$$q^{\mathrm{L}} = q_{i,j} + \left\{ \left(\frac{s}{4}\right)[(1 - \kappa s)\Delta_- + (1 + \kappa s)\Delta_+]q \right\}_{i,j} \tag{6}$$

$$q^{\mathrm{R}} = q_{i+l,j} - \left\{ \left(\frac{s}{4}\right)[(1 + \kappa s)\Delta_- + (1 - \kappa s)\Delta_+]q \right\}_{i+l,j} \tag{7}$$

Limiters need to be used in order to eliminate spurious wiggles at discontinuities, such as shock waves. In this paper, we have used a slope limiter, s as given below.

$$s = \frac{2(\Delta_+ Q)(\Delta_+ Q) + \varepsilon}{(\Delta_+ Q)^2 + (\Delta_- Q)^2 + \varepsilon}, \quad \text{where } \varepsilon \approx 10^{-7}. \tag{8}$$

The numerical time integration is carried out by either a Runge-Kutta four stage scheme or an implicit scheme (Qin *et al.*, 2000).

2.3.3 Boundary conditions. At the far field boundaries, characteristic boundary conditions are applied. In the present study of two-dimensional flows over aerofoils, this implies either a subsonic inflow or a subsonic outflow characteristic boundary condition.

At the aerofoil surface without mass transfer, a no-slip boundary condition is specified. At the surface with mass transfer, the normal velocity component is determined by

$$v_{\mathrm{w}} = \frac{C_Q \rho_\infty U_\infty c}{\sum\limits_{L_{\mathrm{suction}}} \rho_{\mathrm{w}} \Delta s}, \tag{9}$$

where the suction/blowing coefficient is defined as:

$$C_Q = \frac{\dot{m}}{\rho_\infty U_\infty c} = \frac{1}{\rho_\infty U_\infty c} \int_{s_1}^{s_2} \rho_{\mathrm{w}} v_{\mathrm{w}} \, \mathrm{d}s. \tag{10}$$

For the relatively weak suction and blowing considered in this study, the viscous boundary conditions can reasonably be applied. In addition to the above normal velocity component, the tangential velocity component is determined from the suction/blowing inclination angle.

2.4 Force calculation and system consideration

In the case of suction, mass is removed from the flow external to the aerofoil surface. Obviously, the same amount of mass has to be ejected somewhere from the aerofoil into the main flow to conserve mass. From the conservation of momentum, or Newton's second law, there will be an additional force acting on the aerofoil in addition to the pressure and skin-friction forces acting on the external surfaces of the aerofoil. However, this force will depend on how the sucked air is ejected into the main flow. These include factors such as where to eject, at what direction and at what speed. The ejection itself in turn will also influence the flowfield and, therefore, pressure and skin-friction forces on the aerofoil. Furthermore, for practical application, it is also necessary to consider the cost for the installation of the pipeline system inside the aircraft, the power required to run the pump and the losses in the pipe system. This highlights the importance of considering the system as a whole for successful implementation of flow control devices involving surface mass transfer.

The current study is limited to the study of the effect of suction control on the flowfield as an isolated factor. Therefore, system integration issues are not discussed further in this paper, although they would obviously have to be investigated in a more general study. It is assumed that the air sucked from the mainstream is ejected out through a pipeline normal to the aerofoil cross section at the pipe exit. Therefore, there is no contribution to the lift and drag forces from the ejected air. Similarly, for the cases of blowing, the present studies are limited only to isolated effects of blowing on the forces acting on the aerofoil.

3. Validation

3.1 NACA64A010 aerofoil with suction

The NACA64A010 aerofoil was tested extensively by Smith and Walker (1960) at transonic conditions with surface suction downstream of the hinge line of the trailing-edge flap. It is a 10 per cent c thick aerofoil, symmetric if the trailing edge flap is not deflected. The NACA six-series wing section was designated for profiles with substantial portion of laminar boundary layers due to favourable pressure gradient.

The flow conditions investigated in the experiment correspond a Reynolds number of 2.9 million based on aerofoil chord for a range of Mach numbers from 0.70 to 0.84 and a range of angles of incidence from -1 to 4°. Both suction parameter and flap angle were varied in the experiments.

The flow conditions chosen for computation were $M_\infty = 0.78$, $\alpha = 0.5°$ and $\mathrm{Re} = 2.9 \times 10^6$ corresponding to one of the wind tunnel experimental conditions. In the experiment, the suction region was located between 69 and 72.5 per cent of chord length from the leading edge, which is downstream of the shock position without suction. The suction coefficient was 0.00225, with a flap deflection of 1°. The suction angle β was chosen to be 84° to the aerofoil surface,

since the suction is normal to the chord line. The flow was assumed to be fully turbulent due to the high Reynolds number in the experiment. The 189×65 grid around the aerofoil is shown in Figure 1 with clustering near the surface, the leading and trailing edges, and the shock wave location.

For quantitative comparison, the pressure distributions from both computation and experiment, with and without suction, are compared in Figure 2. These figures show that the computation is in good agreement with the experimental data in both cases. The effect of the surface suction is captured quite well. The Mach contours (Figure 3) show the effects of suction on increasing the shock strength.

Table I shows the comparison of the lift and drag coefficients for the NACA64A010 aerofoil cases for a fixed incidence. The comparison between the experimental data and the computed results is reasonably good. However, in comparison with a rather good agreement in pressure distribution, the discrepancies are a little disappointing, which may be due to the grid sensitivity of the computation or the uncertainties in the experiments.

One can observe from the results that, for the present suction control downstream of the shock wave, both lift and drag are increased with a more substantial increase in the lift. These increases can be explained in the

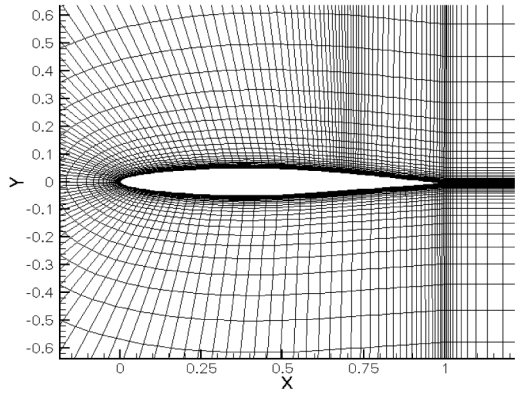

Figure 1.
NACA64A010 case grid

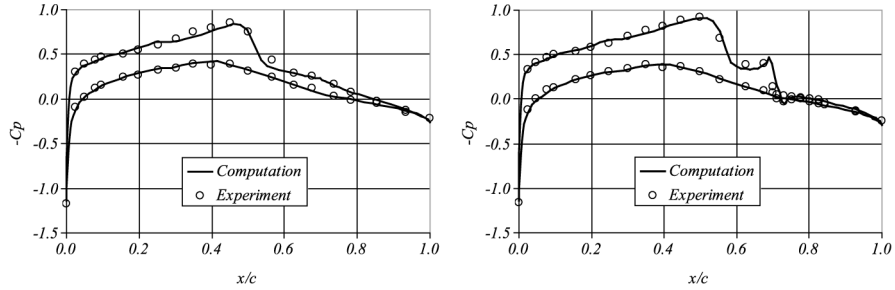

Figure 2.
Surface pressure distribution around NACA64A010 aerofoil: no suction (left) and with suction (right)

following analyses of the suction's effects on the boundary layers and the skin-friction.

Figure 4 shows the predicted boundary-layer displacement thickness, δ^*, both with and without suction. It shows that the displacement thickness has a sudden increase under the shock wave. Upstream of the shock, suction has little effect on the displacement thickness, except that the shock is displaced slightly downstream. Immediately downstream of the shock, the displacement thickness is increased by the suction, but only after a small distance further downstream this drops down below the corresponding "no-suction" value on

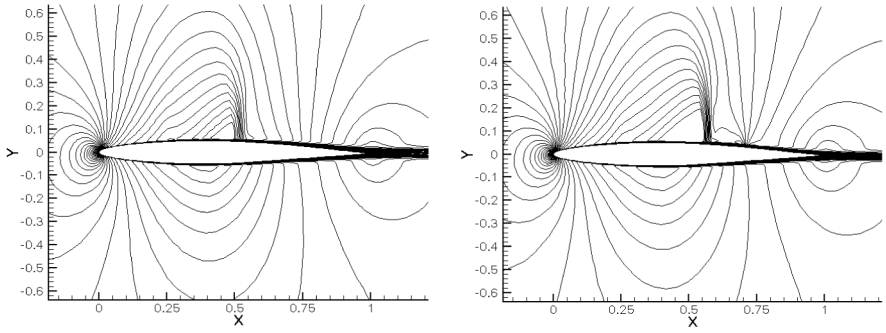

Figure 3.
Mach contours around NACA64A010 aerofoil: no suction (left) and with suction (right)

	C_L	C_D
No suction		
Experiment	0.20	0.013
Computation	0.2166	0.0111
With suction		
Experiment	0.24	0.014
Computation	0.2795	0.0138

Table I.
NACA64A010 aerofoil lift and drag coefficient without and with suction

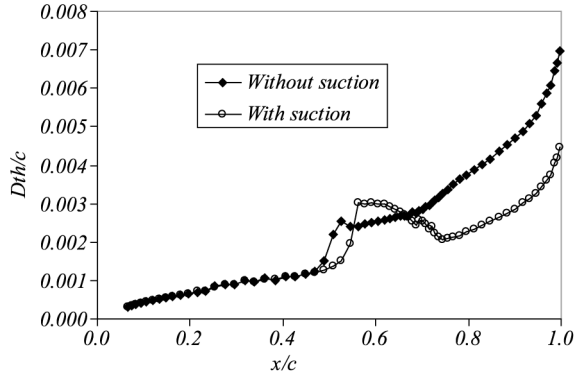

Figure 4.
Computed boundary-layer displacement thickness on NACA64A010 aerofoil

the last third of the aerofoil downstream of the suction region. This indicates that the suction increases the effective camber of the aerofoil and therefore the lift, shown earlier.

The skin-friction distributions on the upper surface of the aerofoil are plotted in Figure 5, for the cases with and without suction. Very high skin-friction over the suction region can be clearly observed, contributing to the skin-friction drag. This higher local skin-friction is due to the higher velocity gradient at the surface as part of the low energy flow in the boundary layer has been sucked in. The local high skin-friction was also observed in experimental tests, e.g. Ashill *et al.* (1996). For both cases, the skin-friction reduces to a value near zero, locally due to the effect of a strong adverse pressure distribution created by the shock wave. Since suction actually strengthens the shock in this case, the skin-friction becomes closer to the incipient separation condition with suction. This indicates that suction downstream can promote shock-induced separation locally (bubble type).

Note that in practical applications and experiments, suction control is mostly achieved through sucking through porous surfaces. In the simulation, this is modelled in the macro scale by distributed surface mass transfer as implemented in the numerical boundary condition (equation (10)). Strictly speaking, the skin-friction is only for the solid part of the porous surface. However, the porosity is practically rather small and therefore the local skin-friction can be reasonably represented by the local shear stress over the solid surface.

3.2 RAE5243 aerofoil with suction

The RAE5243 aerofoil with a maximum thickness-chord ratio of 14 per cent is a natural laminar flow (NLF) aerofoil with a pressure distribution on the upper surface having a favourable pressure gradient upstream of the shock at about 55 per cent chord. The aerofoil has a very slight blunt trailing edge (0.5 per cent c). The flow conditions were $M_\infty = 0.6799$, $\mathrm{Re} = 18.68 \times 10^6$, corresponding to the wind tunnel experiment by Fulker and Simmons (1994). The angles of incidence measured in the experiment for both cases (with and without suction) to be studied are $\alpha = 0.77°$. The suction region is located at 45-46 per cent chord

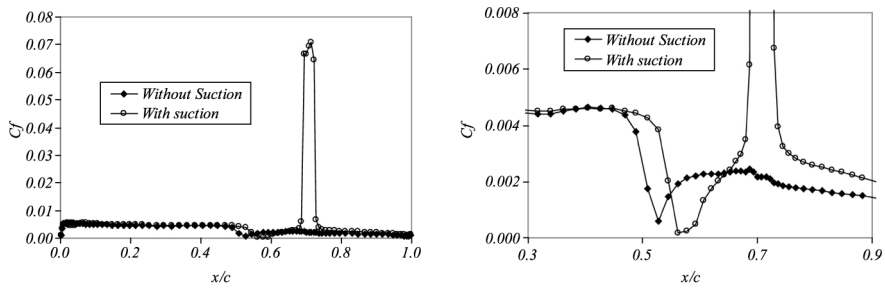

Figure 5.
Computed skin-friction distributions on NACA64A010 aerofoil: overview (left) and local (right)

length with suction coefficient $C_Q = 9 \times 10^{-5}$ and the suction angle $\beta = 89°$. It is a case of weak suction about 10 per cent chord upstream of the shock wave.

Initial studies revealed that a proper treatment of the trailing edge in the numerical model is crucial for the accurate prediction of aerofoil lift and drag. A multi-block solution approach has to be adopted to provide a precise simulation of the trailing edge flow although the bluntness is only 0.5 per cent chord. The grid is generated in two blocks, one around the aerofoil (189×65) and the other in the wake region (25×47) that is behind the blunt trailing edge as shown in Figure 6.

Computational and experimental pressure distributions for the RAE5243 aerofoil are shown in Figure 7, for cases without and with suction, respectively, at the same experimental normal force coefficient. The figures show that the computation is in excellent agreement with the experimental data for both cases. Note that the trailing edge pressure is slightly open due to the slight bluntness of the trailing edge.

Table II shows the lift and drag comparison between the experiment and the computation. One can observe an excellent agreement in lift while some discrepancies in drag remains. Unlike the previous case, the effects of suction are rather small, reducing both very slightly.

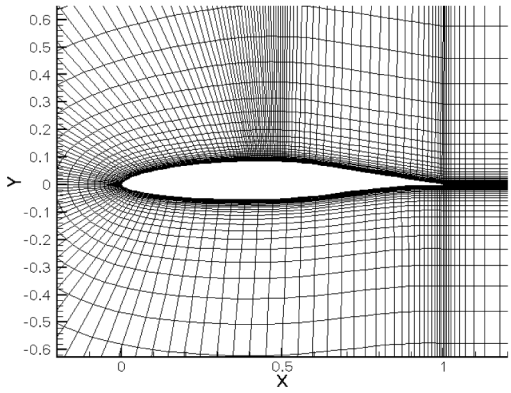

Figure 6.
RAE5243 two-block grid

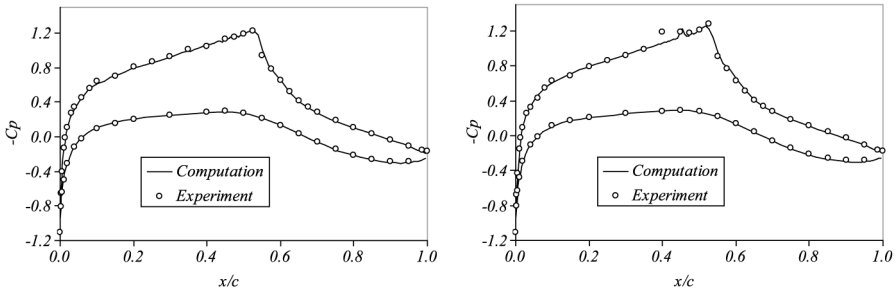

Figure 7.
Surface pressure distribution around RAE5243 aerofoil: no suction (left), suction (right)

Figure 8 shows the Mach number contours for the case with suction. The perturbation of the flowfield by suction can be seen ahead of the shock wave. However, this does not have an effect on reducing the shock's strength. This is also evident in the surface pressure distribution (Figure 7).

3.3 RAE5225 aerofoil with surface bump

The RAE5225 aerofoil is a supercritical aerofoil with a maximum thickness to chord ratio of 14 per cent. The characteristics of a supercritical aerofoil are quite different from those of an NLF aerofoil. While the NFL aerofoil tries to maintain a favourable pressure gradient to stabilise the boundary layer, the supercritical aerofoil is designed to delay the drag rise Mach number, which results in a much earlier onset of an adverse pressure gradient on the aerofoil.

The flow conditions chosen for the computational test were $M_\infty = 0.734$ and $\mathrm{Re} = 6.1 \times 10^6$ with transition fixed at 5 per cent chord on both upper and lower surfaces corresponding to the wind tunnel experiment by Fulker *et al.* (1993). A bump of circular-arc shape and of maximum height (relative to the upper surface of the datum aerofoil) of 0.175 per cent chord was fixed at 40-60 per cent chord position on the upper surface as shown in Figure 9 along with the grid.

Figure 10 shows the computational and the experimental pressure distributions for the RAE5225 aerofoil with 0.175 per cent chord length height bump at 40-60 per cent chord length from the leading edge at 2.95°

	C_L	C_D
No suction		
Experiment	0.5154	0.0877
Computation	0.5142	0.0980
With suction		
Experiment	0.5146	0.0830
Computation	0.5144	0.0968

Table II.
RAE5243 aerofoil lift and drag coefficient without and with suction

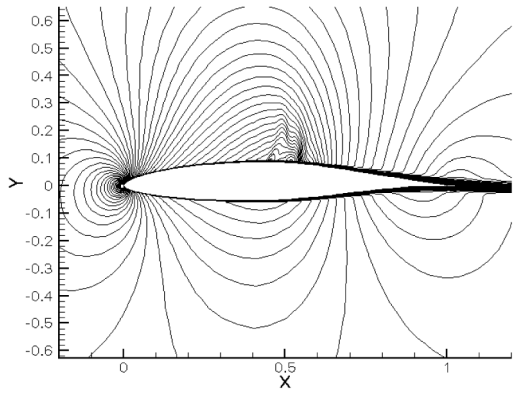

Figure 8.
Mach contours for RAE5243 suction case

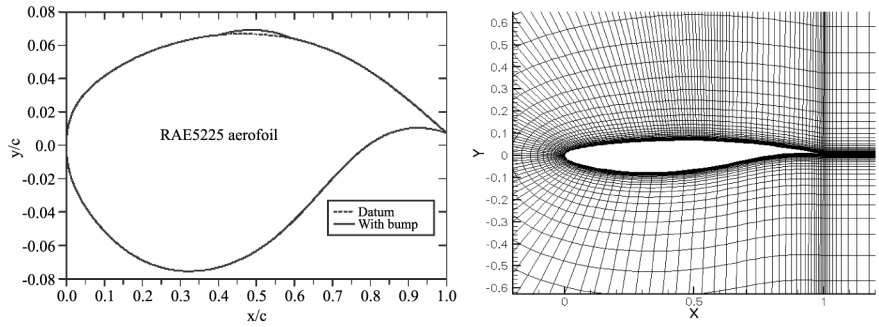

Figure 9.
RAE5225 aerofoil with bump and grid

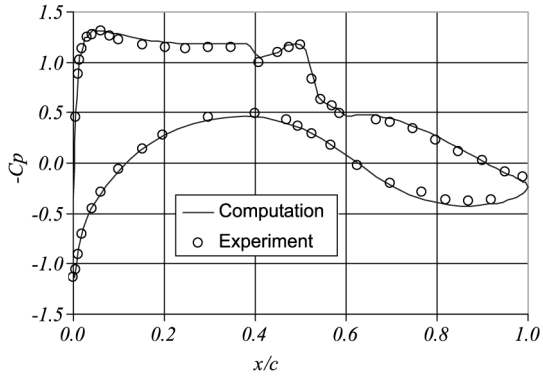

Figure 10.
Surface pressure distribution around RAE5225 aerofoil with surface bump

incidence. It shows that the computation is in good agreement with the measurement.

Table III shows the comparison of the computation with the experimental data for the given incidence of 2.95°. The difference between the lift, between the experiment and computation may come from the wall interference of the wind tunnel test, which generally has an effect of reducing the effective incidence of the aerofoil (Zhu, 2000). A more useful comparison for the force coefficient data is to compare the drag for a given lift coefficient. A reasonable comparison can then be achieved.

Figure 11 shows the flowfield in Mach number contours. It is clear that the compression waves ahead of the shock wave have the effect of reducing the shock strength and therefore the wave drag. The mechanism of the drag reduction is due to the reduction of the shock strength and the wave drag. It is

	C_L	C_D
Experiment	0.7200	0.0150
Computation	0.7523	0.0172

Table III.
RAE5225 aerofoil lift and drag coefficient with bump

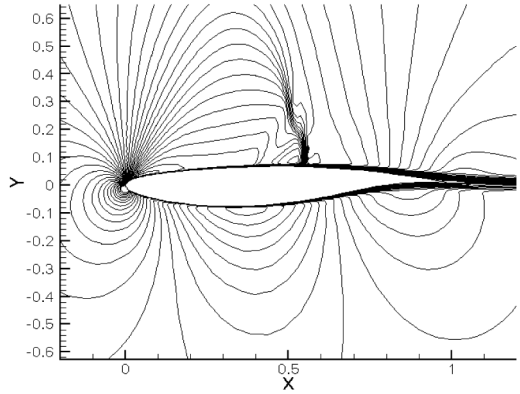

Figure 11.
Mach contours for RAE5225 aerofoil bump case

therefore concluded that the control is achieved through the inviscid flow behaviour rather than the viscous effects. Indeed, Euler solutions indicate that a more significant drag reduction can be achieved and the viscous effects tend to moderate such reductions and therefore the effectiveness of the bump control device.

4. Parametric studies

In this section, we study the influence of some parameters in the various control devices in order to identify the key ones affecting the aerodynamic performance of the aerofoil.

4.1 Suction

The effect of the position of suction regions relative to the shock position is shown in Figures 12 and 13 for the RAE5225 aerofoil case, where $M_\infty = 0.734$, $\alpha = 3°$ (for Figure 12 only), $C_Q = 5 \times 10^{-4}$. Apparently, suction changes the local pressure significantly. The aerofoil performance can be improved by suction located at or downstream of the shock position. However, when the

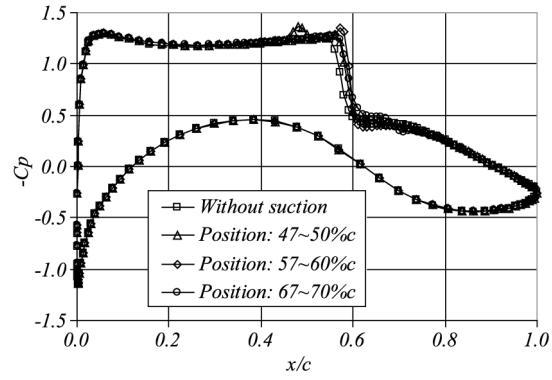

Figure 12.
Pressure distribution around RAE5225 aerofoil – effect of suction position at $M_\infty = 0.734$, $\alpha = 3°$

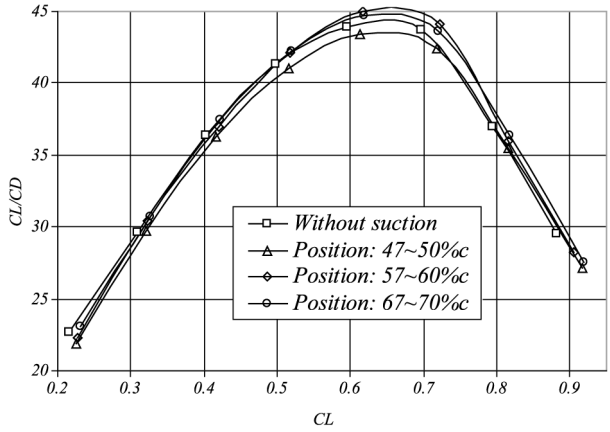

Figure 13.
Lift-drag ratio for RAE5225 aerofoil – effect of suction position

suction position is upstream of the shock position, the aerodynamic performance is degraded (Figure 13). This behaviour is consistent with the detailed analysis in Section 3. For a given incidence, suction downstream of the shock location has the effect of increasing both lift and friction drag but the L/D ratio is generally improved due to a more significant increase in lift. However, suction upstream of the shock wave has a relatively small effect on the lift but with a similar skin-friction penalty, which explains the degradation of the aerodynamic performance.

The suction strength also has a strong effect on the aerofoil surface pressure distribution and the L/D ratio. Figures 14 and 15 show the results for $M_\infty = 0.734$, $\alpha = 3°$ (for Figure 14 only) and suction position at 67-70 per cent c, downstream of the shock. Increasingly, stronger suction has an effect of pulling the shock further downstream (Figure 14) and shifting the L/D ratio curve to the right into the higher lift region (Figure 15). This indicates that while stronger

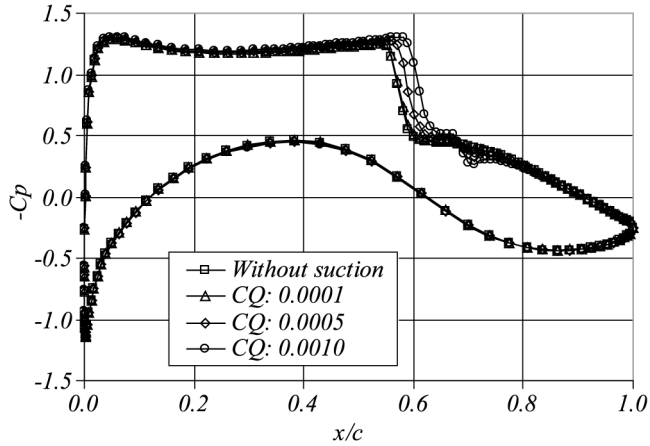

Figure 14.
Pressure distribution around RAE5225 aerofoil – effect of suction mass flow at M_∞=0.734, $\alpha = 3°$

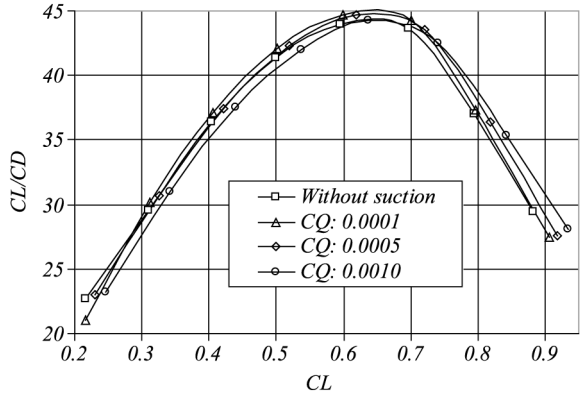

Figure 15.
Lift-drag ratio for RAE5225 aerofoil – effect of suction mass flow

suction can improve the performance in the high lift region, the performance in the low lift region can be degraded. For the relatively weaker suction, there is only a slight improvement around $C_L = 0.65$. The results indicate a strong dependency of the suction strength design on the design lift condition.

4.2 Blowing

As shown in Section 3, a local bump can improve the aerodynamic performance by moderating the shock wave on the upper surface of the aerofoil at transonic speeds. Similar effects may also be expected by blowing at the foot of the shock wave. It can thicken the local boundary layer so as to increase the boundary layer displacement. This in turn forms an effective local air ramp to moderate the shock wave by pre-compression (isentropic).

Three blowing positions, 45-50 per cent chord, 50-55 per cent chord, and 55-60 per cent chord near the foot of the shock wave, were selected to investigate the effects of the blowing position. The case is for $M_\infty = 0.68$, $C_Q = 4 \times 10^{-4}$, and the inclined blowing angle $\beta = 15°$. Figure 16 shows the aerofoil pressure distributions for three blowing positions at the same

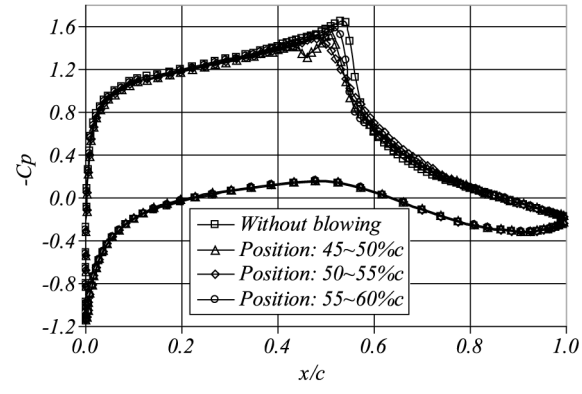

Figure 16.
Surface pressure distribution around RAE5243 aerofoil – effect of blowing position

incidence $\alpha = 3°$. It clearly shows that blowing changes the pressure distribution. The shock strength is reduced, and the shock wave moves upstream, the effect being particularly apparent when blowing is right underneath the shock wave. It is interesting to see that blowing slightly downstream of the original shock wave can also slightly reduce the shock strength by moving it upstream. Blowing at 50-55 per cent under the shock (at ~55 per cent) is most effective in reducing the shock strength with a similar effect as the solid bump.

Figures 17 and 18 show the boundary layer behaviour and the skin-friction with and without blowing. The blowing case is for the 50-55 per cent c position. They show that blowing increases the boundary-layer thickness and reduces the skin-friction drag for a fixed incidence. These are both due to the effect of

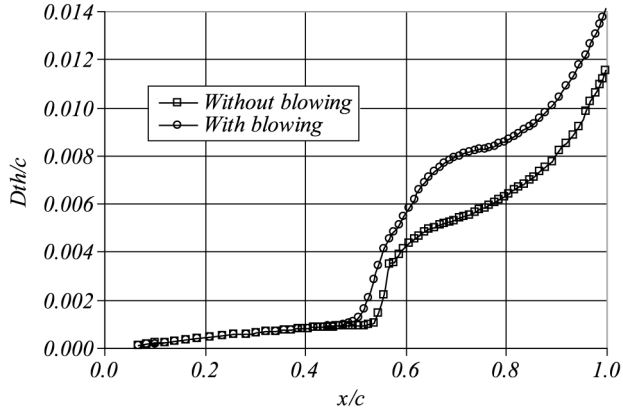

Figure 17.
Computed boundary-layer displacement thickness for RAE5243 aerofoil

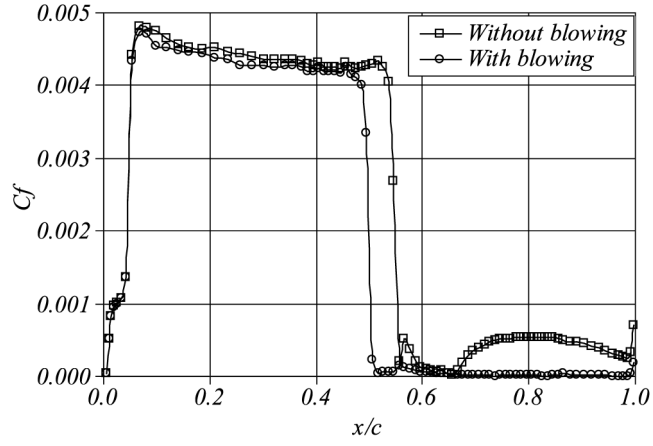

Figure 18.
Computed skin-friction for RAE5243 aerofoil

the blowing pushing the boundary layer outward, reducing the velocity gradient at the wall in the process.

Figure 19 shows the lift-drag ratio plotted against lift coefficient for the blowing cases, which reveals that the blowing reduces the lift-drag ratio significantly over the whole range of the lift coefficients studied, although the shock wave is weakened. The behaviour is in total contract with the suction cases, where the shock strength is increased with an increase in the lift-drag ratio.

The effects of the blowing angle were studied by investigating three inclination angles, 5, 15 and 45° with other parameters fixed. The angle is defined as the angle between the blowing flow direction and the local aerofoil surface tangent. The results were hardly distinguishable. This indicates that in the present investigation, the blowing control effects are from the effects of the mass flow injection and the boundary layer thickness change instead of the effects of the momentum injection (as often used to energize the boundary layer).

Blowing further away from the shock wave has also been studied for the RAE5225 aerofoil. It was found that appropriate blowing could increase the lift-drag ratio. Blowing near the trailing edge with small blowing coefficient indicated some improvement in L/D for the RAE5225 aerofoil. The blowing position in these calculations was taken to be near the trailing edge at 97.5-98 per cent chord, with the blowing coefficients $C_Q = 0.0005$ and 0.001 and $\beta = 5°$.

Figure 20 shows the pressure distributions for the RAE5225 aerofoil for $\alpha = 3°$ with blowing near the trailing edge. It shows that blowing far away the shock wave weakly can also weaken the shock wave, and move the shock wave upstream slightly. Figure 21 shows the lift-drag ratio against lift coefficient for the corresponding cases. It shows that weak blowing near trailing edge with

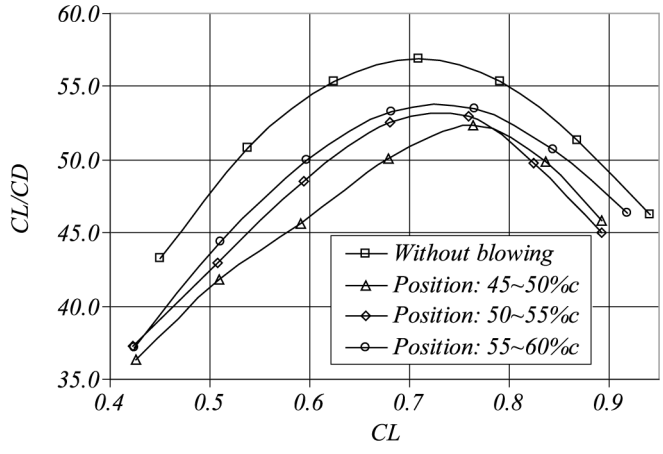

Figure 19.
Lift-drag ratio for RAE5243 aerofoil – effect of blowing position

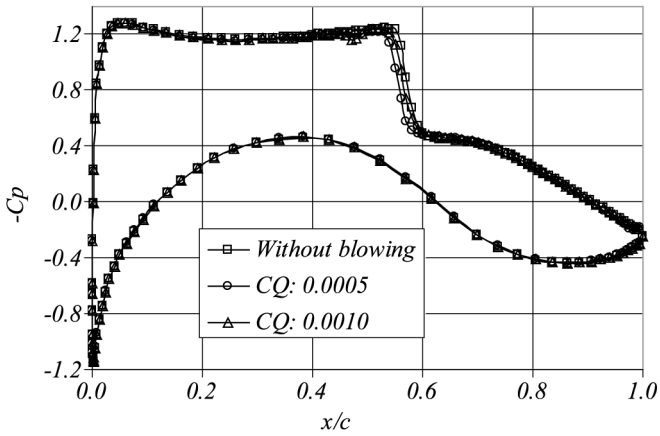

Figure 20.
Pressure distribution for RAE5225 – near trailing edge blowing

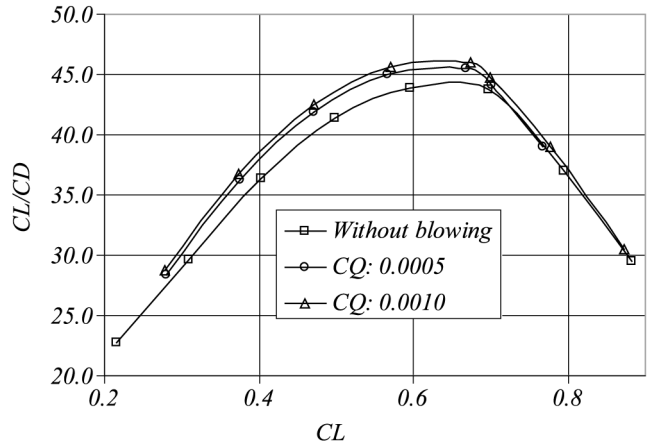

Figure 21.
Lift-drag ratio for RAE5225 – near trailing edge blowing

a small angle to the aerofoil surface can improve the aerodynamic performance of the aerofoil for $C_L < 0.7$. It is most beneficial in the maximum lift-drag ratio region. There is very little improvement for higher lift region. Unlike the suction and bump cases, this improvement is related to the modification of the trailing edge flow (similar to the jet flap for increasing circulation) rather than the near shock behaviour.

4.3 Surface bumps

Figure 22 shows the RAE5243 aerofoil datum section with 0.175 per cent chord high bump at 40-60 per cent chord. The bump is made of a circular arc, similar to Fulker *et al.* (1993), on top of the original datum aerofoil. The flow conditions are $M_\infty = 0.68$, $\mathrm{Re} = 19 \times 10^6$ with transition fixed at 5 per cent chord on both upper and lower surfaces. Figures 23 and 24 show the pressure distributions

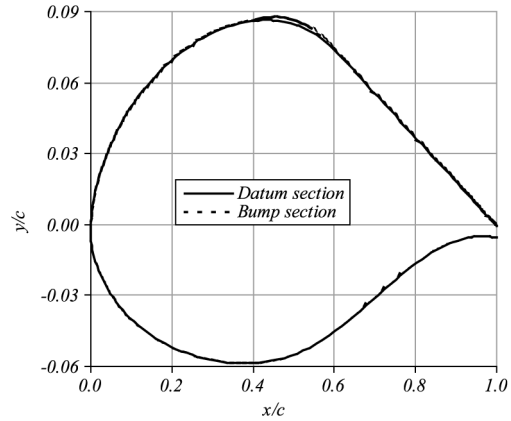

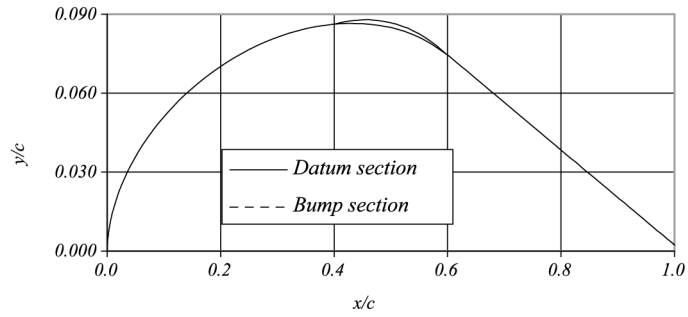

Figure 22.
RAE5243 aerofoil with bump

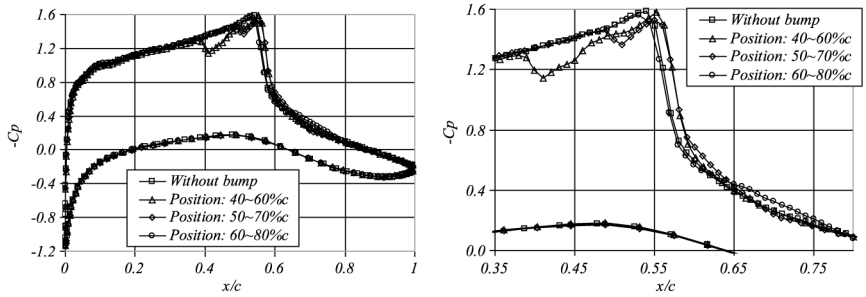

Figure 23.
Surface pressure distribution around RAE5243 aerofoil – effect of bump position

for the RAE5243 aerofoil at an angle of incidence $\alpha = 2.5°$, for three bump positions. The figure demonstrates the sensitivity of the pressure distribution to the bump location. When placed with its crest close to the shock the bump can serve well the purpose of reducing shock strength and hence wave drag.

It is particularly interesting to examine the effect of bump positions on L/D for a wide range of lift coefficients, as shown in Figure 24. This figure shows

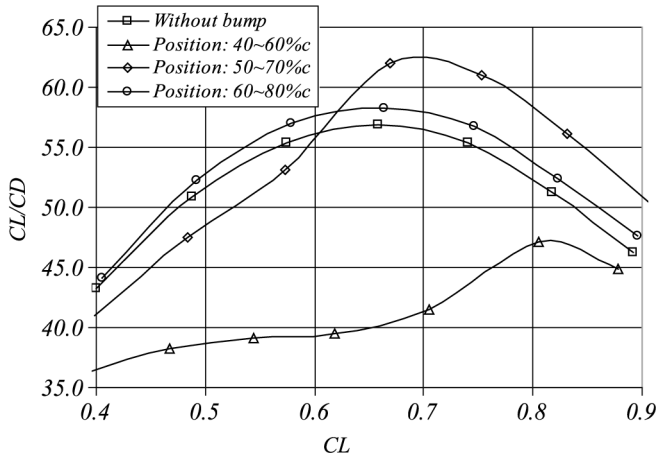

Figure 24.
Lift-drag ratio for RAE5243 aerofoil – effect of bump position

that a bump at 40-60 per cent chord (ahead of the shock) reduces the L/D ratio for the whole lift range considered, while a bump at 60-80 per cent chord (downstream the shock) increases the lift-drag ratio moderately over the same lift range. A bump at 50-70 per cent chord (under the original shock) increases the lift-to-drag ratio significantly for the high lift region but degrades the performance of the original aerofoil at the lower lift region (0.4-0.6). There is an interesting crossover at $C_L = 0.6$. Note that for NLF aerofoil the shock position is almost fixed at 55 per cent for the incidence (lift) range considered.

Another important parameter is the bump height as shown in Figure 25. This shows results for three different bump heights located at 50-70 per cent for the RAE5243 aerofoil. It demonstrates that the higher bump gives more significant gain at higher lift range and, at the same time, more degradation at the lower lift range. This can be attributed to the fact that higher lift cases

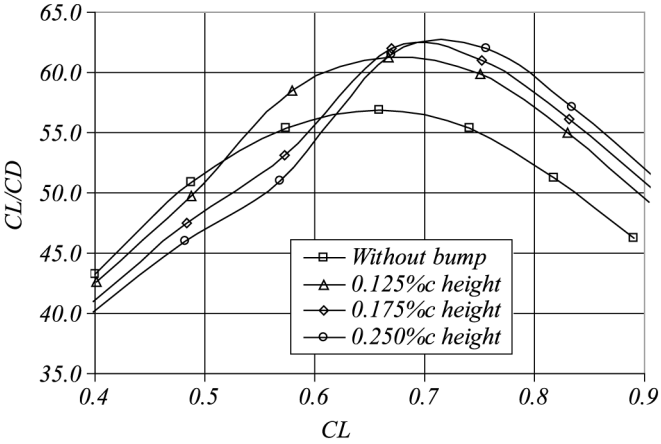

Figure 25.
Lift-drag ratio for RAE5243 aerofoil – effect of bump height (position: 50-70 per cent)

correspond to stronger shock waves. Higher bumps have a stronger effect in reducing the shock strength and therefore, the wave drag. We can also conclude from the results that the higher bump (0.25 per cent c) serves better as a device for delaying drag rise or buffet onset. However, for a wider operational range for beneficial effects, a lower bump (0.125 per cent c) may be better for both drag reduction and buffet delay.

5. Conclusions

A numerical study is presented based on a high-resolution solution of the Reynolds averaged Navier-Stokes equations using an algebraic turbulence model with surface mass transfer effects. Some validation work has been presented against available experimental data regarding surface pressure distribution and lift and drag coefficients.

A parametric study of shock control for transonic aerofoil flows using suction, blowing, and local changes to the local surface contour has been carried out.

Suction generally improves the aerofoil transonic aerodynamic performance through an increased lift-drag ratio. It achieves this, despite the tendency for suction to increase shock strength, while moving the shock wave downstream (indicative of an increase in wave drag). It was noted that the associated increase in lift is generally more than that in drag. However, as a shock control device, suction is ineffective in reducing the shock strength and the associated wave drag.

Blowing ahead of the shock was found to reduce the shock strength significantly by creating a λ-shock structure or a compression fan. Blowing downstream of the shock can also move the shock upstream and reduce the shock strength slightly. The angle of inclination of blowing has shown little effect on the control, with smaller angles showing a slightly better performance. Drag polars indicate that blowing near the foot of the shock (either just upstream or just downstream of the shock) does not provide a reduction in drag for a given lift. However, weak blowing near the trailing edge can improve the performance before the drag rise.

Bumps placed in the vicinity of the shock reduce shock strength and wave drag significantly with no substantial increase in viscous drag. The result is a significant increase in lift/drag ratio and a delay in buffet onset, confirming previous studies at DERA. The physical mechanisms for the improvement are highlighted by the flowfield simulations and provides further insight into the nature of the local flow interactions in the region of the shock. This provides the basis for optimising the bump arrangement. Among the three devices investigated, the bump is the only one that achieves a total drag reduction at a given lift condition through weakening the shock wave strength, giving the best performance. It can serve as a fixed device to an existing aerofoil or as an adaptive deployable device when required. Since the lower bump has a

relatively wider operational range, it may be used as a fixed device. On the other hand, active bumps may be adapted for best performance for the given operational point. Potential ideas for such bumps may be achieved by recent development in shape memory alloy diaphragms, piezoelectric patches and small inflatable blisters.

In practical applications, for all the shock control devices, the benefits need to be weighed against the cost associated with the devices through system integration studies. In this regard, controls involving surface mass transfer (both suction and blowing) may be more complicated and therefore more costly as compared to the bumps.

References

Ashill, P.R. and Fulker, J.L. (1999), "A review of flow control research at DERA", Private Communication.

Ashill, P.R., Fulker, J.L., Simmons, M.J. and Gaudet, I.M. (1996), "A review of research at DRA on active and passive control of shock waves", *Proceedings of the International Congress in Aeronautical Sciences*.

Baldwin, B.S. and Lomax, H. (1978), "Thin layer approximation and algebraic model for separated turbulent flows", AIAA Paper 78-0257.

Cebeci, T. (1970), "Behaviour of turbulent flow near a porous wall with pressure gradient", *AIAA J.*, Vol. 8 No. 12, pp. 2152-6.

Chen, C.L., Chow, C.Y., William, R. and Holst, T.L. (1989), "Computation of viscous transonic flow over porous airfoils", *J. Aircraft*, Vol. 26 No. 12, pp. 1067-75.

Delery, J.M. (1985), "Shock wave/turbulent boundary layer interaction and its control", *Progress in Aerospace Sciences*, Vol. 22 No. 4, pp. 209-80.

Delery, J.M. (1999), "Shock phenomena in high speed aerodynamics: still a source of major concern", *Aeronautical J.*, Vol. 103 No. 1019, pp. 19-34.

Fulker, J.L., Ashill, P.R. and Simmons, M.J. (1993), "Study of simulated active control of shock waves on aerofoil sections", DRA Technical Report TR93025.

Fulker, J.L. and Simmons, M.J. (1994), "An experimental study of shock control methods", RA/AS/HWA/TR94007/1.

Pearcey, H.H. (1961), "Shock-induced separation and its prevention by design and boundary layer control", *Boundary Layer and Flow Control*, Pergamon Press, New York, NY, Vol. 2.

Qin, N., Ludlow, D.K. and Shaw, S.T. (2000), "A matrix-free preconditioned Newton/GMRES method for unsteady Navier Stokes solutions", *International Journal of Numerical Methods in Fluids*, Vol. 33 No. 3, pp. 223-48.

Qin, N. and Zhu, Y. (1999), "Inclined suction and blowing for shock control at transonic speeds", *Proceedings of the 22nd International Symposium on Shockwaves*, London.

Qin, N., Zhu, Y. and Poll, D.I.A.P. (1999), "Surface suction on aerofoil aerodynamic characteristics at transonic speeds", *Proceedings of IMechE Part.G J. Aeronautical Engineering* Vol. 212, pp. 339-51.

Regenscheit, B. (1941), "Drag reduction by suction of the boundary layer separated behind shockwave formation and high Mach numbers", NACA TM 1168.

Smith, D.W. and Walker, J.H. (1960), "Test of an area suction flap on a NACA64A010 airfoil at high subsonic speeds", NASA TN D 310.

Wong, W.F. (1977), "Application of boundary layer blowing to suppress strong shock induced separation in a supersonic inlet", AIAA Paper 77-147.

Zhu, Y. (2000), "Computational study of shock control at transonic speed", PhD thesis, College of Aeronautics, Cranfield University.

Zhu, Y. and Qin, N. (1999), "Inclined slot blowing on transonic aerodynamics performance of the RAE 5243 and RAE 5225 aerofoils", CoA Report 9906, Cranfield University.

Further reading

Amitay, M. and Honohan, A. (1997), "Modification of the aerodynamic characteristics of bluff bodies using fluidic actuators", AIAA 97-2004.

Osher, S. and Solomon, F. (1982), "Upwind difference schemes for hyperbolic systems of conservation laws", *Mathematics of Computation*, Vol. 38 No. 158, pp. 339-74.